IOPscience iopscience.iop.org

Home Search Collections Journals About Contact us My IOPscience

Characterization of defect levels in semi-insulating 6H-SiC by means of photoinduced transient spectroscopy and modulated photocurrent technique

This article has been downloaded from IOPscience. Please scroll down to see the full text article.

2009 J. Phys.: Condens. Matter 21 045801

(http://iopscience.iop.org/0953-8984/21/4/045801)

View the table of contents for this issue, or go to the journal homepage for more

Download details:
IP Address: 129.252.86.83
The article was downloaded on 29/05/2010 at 17:30

Please note that terms and conditions apply.

J. Phys.: Condens. Matter **21** (2009) 045801 (14pp) doi:10.1088/0953-8984/21/4/045801

# Characterization of defect levels in semi-insulating 6H-SiC by means of photoinduced transient spectroscopy and modulated photocurrent technique

**C Longeaud**[1], **J P Kleider**[1], **P Kaminski**[2], **R Kozlowski**[2] **and M Miczuga**[3]

[1] Laboratoire de Génie Electrique de Paris, CNRS (UMR 8507), Ecole Supérieure d'Electricité, Universités Paris VI et XI, 11 rue Joliot Curie, Plateau de Moulon, F-91192 Gif sur Yvette Cedex, France

[2] Institute of Electronic Materials Technology, 133 Wolczynska Street, PL-01919 Warsaw, Poland

[3] Military University of Technology, 2 Kaliskiego Street, PL-00908 Warsaw, Poland

E-mail: longeaud@lgep.supelec.fr

Received 20 October 2008
Published 22 December 2008
Online at stacks.iop.org/JPhysCM/21/045801

**Abstract**

Parameters of electrically active defect centres in vanadium-doped 6H silicon carbide (6H-SiC:V) were investigated by means of the photoinduced transient spectroscopy (PITS) and modulated photocurrent (MPC) method. After a short description of the two techniques, experimental results are presented and briefly compared. Our aim is mainly to understand and explain these experimental results. In particular, in the PITS technique a shallow level seems to be at the origin of negative photoconductivity. Besides, in the same temperature range hole and electron levels can be detected at the same time. Finally, the detection of a given level seems to depend on the photon flux used to perform the PITS experiment. As far as the MPC experiment is concerned, it has put into evidence a very efficient shallow level. A numerical calculation was developed to simulate both experiments in order to understand the experimental results. By means of this simulation, we have explained all the phenomena observed experimentally in each technique and we propose a simple model for the distribution of electrically active defect centres in 6H-SiC:V crystals.

(Some figures in this article are in colour only in the electronic version)

## 1. Introduction

Investigation of defects in semiconductors is of primary importance to tailor these materials for a given application. Indeed, these defects are responsible for the electronic (e.g. conductivity, lifetime) and optical (e.g. luminescence, absorption) properties of semiconductors. In this paper we concentrate on the investigation of defect centres present in vanadium-doped 6H silicon carbide (6H-SiC:V) crystals. This wide bandgap material finds some applications as a substrate for the growth of InGaN epitaxial layers for instance, but it is also a very promising material for electronics operating in hard environments (e.g. high temperature) or for high power output. Detection and determination of the parameters (e.g. concentration, energy position, capture cross section) of the defect levels introduced, deliberately or not, during the crystal growth is of primary importance, for it is these levels that fix the photoelectronic behaviour of the crystal and consequently the possible applications. Our investigations were performed by means of two different techniques: the photoinduced transient spectroscopy (PITS) and the modulated photocurrent (MPC) method. Both techniques take advantage of the photoconductivity of the material and how it is influenced by levels in the bandgap. These two techniques

 © 2009 IOP Publishing Ltd Printed in the UK

were used to investigate defect levels in a wide variety of materials either crystalline [1–5], or amorphous [6]. Their applications to 6H-SiC:V crystals raised some questions such as, among others, the apparent possibility with the PITS technique to observe under the same photon flux and in the same temperature range both a level close to the valence band and a level close to the conduction band. In this paper we expose some of the questions raised by the results of each experiment and try to answer these questions by means of a numerical simulation.

In section 2, the experimental methods are briefly described and we give some details about the experimental procedures for doing both experiments. In section 3 we present some experimental results obtained on 6H-SiC crystals and show that parameters of different defect centres, introducing localized states in the bandgap, can be derived. A tentative attribution of these centres to particular native point defects and impurities is also proposed. In section 4 we present a numerical simulation of transient and modulated photoconductivity to explain the observed experimental results.

## 2. Experiments

### 2.1. The PITS experiment

The PITS experiment was proposed in the late 1970s by Hurtes *et al* [1] for the study of deep levels in semi-insulating GaAs. The crystal, onto which two parallel ohmic electrodes have been deposited, is put under vacuum onto the cold finger of a cryostat. Biased with a dc voltage at a given temperature $T$, it is illuminated with a pulse of high flux of light of wavelength $\lambda$, generating carriers by band to band transitions. The pulse width can be adjusted and is typically of the order of a few milliseconds. After the light is turned off, the photocurrent relaxation waveform is recorded for analysis. Usually the photocurrent relaxation is composed of two parts: a fast decrease linked to recombination of the excess free carriers followed by a slower decrease when the emission towards the bands of carriers from defect states slows down the influence of recombination and thus the decrease of the free carrier concentrations. If one assumes that electrons are the majority carriers, the 'standard' method to determine the electron trapping level energy positions from this relaxation is based on the assumption that the current transient $I(t)$ due to the change in trap occupancy is given at a time $t$ by [4]:

$$I(t) = \sum_j I_j(T) = \sum_j K_j e_{nj}(T) \exp(-e_{nj} t). \quad (1)$$

In this equation $K_j = n_{toj}(T)\mu_n(T)\tau_n(T)s(\lambda, T)q\xi$, where $n_{toj}$ is the initial density of electrons captured by the $j$th trap, $\mu_n$ is the electron mobility, $\tau_n$ is the lifetime of free electrons, $s$ is the effective cross section of the region through which the current is flowing, $q$ is the absolute value of the electron charge and $\xi$ is the applied electric field. The emission rate of the trapped electrons is given by

$$e_n = \nu_n \exp(-E_a/k_b T) = \gamma_n \sigma_n T^2 \exp(-E_a/k_b T), \quad (2)$$

in which $k_b$ is the Boltzmann constant, $E_a$ is an activation energy, usually equal to the energy position of the defect level referred to the conduction band edge, $\nu_n$ is the attempt-to-escape frequency, $\sigma_n$ is the electron capture cross section of the trap and $\gamma_n$ is a material-dependent parameter linked to the equivalent density of states $N_c$ at the conduction band edge. At a given temperature $T_j$ the photocurrent relaxation is analysed using a multi-window approach, a given time window $[t_i, t_{i+1}]$ being delimited by the two times $t_i$ and $t_{i+1}$. For each time window, the PITS function is defined as

$$S(t_i, t_{i+1}, T) = [I(t_i, T) - I(t_{i+1}, T)]/I(0, T), \quad (3)$$

where $I(0, T)$ is the value of the photocurrent pulse at temperature $T$ just before the light is switched off. According to equation (1), $S$ is a sum, $\sum_j S_j(t_i, t_{i+1}, T)$, corresponding to the contribution of various trap levels. For a given trap level $j$, and for a given time window, the plot of $S_j$ versus $T$ exhibits a maximum at a temperature $T_{j,\max}$ at which the thermal emission rate is $e_{nj,\max}$. Since the temperature dependence of $K_j$ in equation (1) is weak compared to the exponential dependence of $e_{nj}$, $T_{j,\max}$ can be obtained easily by differentiating $S_j$ with respect to $e_{nj}$ and setting the result equal to zero, which yields

$$\exp[-e_{nj,\max}(t_{i+1} - t_i)] = \frac{1 - e_{nj,\max} t_i}{1 - e_{nj,\max} t_{i+1}}. \quad (4)$$

Equation (4) can be solved numerically to obtain the dependence of $e_{nj,\max}$ on $t_i$ and $t_{i+1}$. Experimentally, the times $t_i$ and $t_{i+1}$ were chosen such that $t_{i+1} = 3t_i$. Then, equation (4) provides a simple relation between $e_{nj,\max}$ and $t_i$: $e_{nj,\max} \approx 1.23/t_i$. Changing $t_i$ will thus lead to changing $T_{j,\max}$ and $e_{nj,\max}$. An Arrhenius plot of $T^2_{j,\max}/e_{nj,\max}$ reveals a straight line, the slope of which is associated with the energy position of the $j$th defect level, and the extrapolation towards $T = 0$ K gives $\sigma_n$ provided $\gamma_n$ is known.

Though more refined multi-window approaches have been proposed [3], some of the authors have shown that the 'standard' approach could be largely improved to lead to high resolution PITS (HRPITS) by means of refined treatments of the signal [7]. It is this approach that we will use in the following. The last methodological point to be underlined is that it is impossible with this technique to know the type of charge carriers contributing to the photocurrent relaxation. Hence, the activation energies deduced from the data treatment cannot be associated to definite positions of the traps in the gap with reference to the valence or the conduction band. It is the comparison of the HRPITS results with those of some other techniques, such as for instance deep level transient spectroscopy (DLTS) or admittance spectroscopy, that allows linking of the deduced activation energy with a particular defect and its energy position in the gap.

Experimentally, for the study of 6H-SiC:V crystals, the time window was moved along $I(t)$, $t_i$ varying from 10 $\mu$s to a few tenth of a second, and the temperature was varied typically from 40 to 700 K using two different cryostats, in order to cover a wide dynamic of emission rates associated with the probed defect levels. The excitation was provided

by a UV pulse using either an HeCd laser emitting at 325 nm or a semiconductor laser emitting at 375 nm. The maximum photon flux was of the order of $10^{18}$ cm$^{-2}$ s$^{-1}$. The photocurrent transients were recorded after amplification with a gain in the range $10^5$–$10^8$ V/A and numerically digitized with a 12 bit resolution before treatment. The bandwidth of the current amplifier is 100 kHz and for the multi-window approach only time values $t_i$ larger than 10 $\mu$s were considered.

### 2.2. The MPC experiment

The MPC experiment was first proposed by Oheda [8] and analysed in detail by Brüggemann *et al* [9], Longeaud *et al* [10] and Hattori *et al* [11]. The sample geometry and experimental system are basically the same as in the PITS technique. The main difference is that the sample is illuminated by a flux of light modulated at an angular frequency $\omega$. The photon energy is chosen such that it is slightly higher than the bandgap of the studied semiconductor. The ac component of the flux $F_{ac}$ being considered as a small perturbation of the dc component of the flux $F_{dc}$ and assuming that one type of carrier is predominant it was shown that the density of states interacting with these carriers can be estimated by recording the modulus of the alternative current $|I_{ac}|$ resulting from the modulated flux as well as its phase shift $\phi$ referred to $F_{ac}$. For a given type of state defined by their capture cross sections for electrons and holes and a density of states (DOS) $N(E)$ (in cm$^{-3}$ eV$^{-1}$), at a given temperature $T$ one can estimate from experimental parameters the quantity $NC/\mu$, $C$ being the capture coefficient for the dominant type of carriers of these states and $\mu$ being the free carrier mobility. This quantity is given by the relation [9, 10]

$$\frac{NC}{\mu} = \frac{2}{\pi k_b T} s(\lambda, T) q G_{ac} \xi \frac{\sin(\phi)}{|I_{ac}|}, \qquad (5)$$

where $G_{ac}$ is the alternative generation rate of free charge carriers. Another estimate of $NC/\mu$ was proposed by Hattori *et al* from the relation [11]

$$\frac{NC}{\mu} = \frac{s(\lambda, T) q G_{ac} \xi}{k_b T} \omega \frac{d}{d\omega} \left( \frac{\cos(\phi)}{|I_{ac}|} \right). \qquad (6)$$

In equations (5)–(6) the quantity $NC/\mu$, which we shall call the reduced DOS (r-DOS) in the following, depends only on experimentally known parameters. The energy scaling is achieved using the equation

$$\Delta E = k_b T \ln(\nu/\omega). \qquad (7)$$

We have written $\Delta E$ because it is impossible to know from the experiment if the predominant carriers are holes or electrons as is the case for the HRPITS technique. Hence, the probed density of states may be $\Delta E$ below (above) the conduction (valence) band if electrons (holes) are the main carriers, giving rise to the alternating photocurrent. The attempt-to-escape frequency $\nu$ has been defined for electrons in equation (2). It can also be written as $C \times N_{eq}$ in which $N_{eq}$ is the equivalent density of states at the conduction or valence band edge, depending on the majority carriers. In the MPC experiment $\nu$ is the only adjustable parameter and it was shown earlier how to adjust this parameter to determine the energy position and capture coefficient of a defect level in crystalline semiconductors [4].

According to equation (7) a DOS spectroscopy can be achieved by varying either $\omega$ at a given temperature or $T$ at a given $\omega$. Actually, experimentally both are being varied in order to cover a larger energy range.

Before entering into experimental details we would like to recall a few points concerning the MPC data. Firstly, both equations (5) and (6) are obtained from integral expressions in which the product of the density of states and a sharply peaked function is included [10, 11]. However, in the case of equation (6) the function is much sharper and narrower than in the case of equation (5). That is why, when studying crystalline semiconductors, the spectroscopy using equation (6) usually gives rise to narrower peaks than with equation (5). However, equation (6) is based on the derivative of an experimental quantity and sometimes leads to noisy r-DOS spectra, especially when the photocurrent is small. This happens when the defect density is quite high. In the following we shall thus present r-DOS spectroscopy results obtained with either equation.

Secondly, equations (5) and (6) are given for one type of states. If several types of states are present and give a contribution to the modulated photocurrent, the $NC/\mu$ deduced from equation (5) or (6) is actually the sum of the different contributions of the different levels and $NC/\mu = \sum_i N_i C_i/\mu$. Obviously, if among all these levels one is predominant, it is the one that will be probed.

Finally, as mentioned above, and as for the PITS technique, it is impossible with the MPC technique to know which type of charge carrier is mainly responsible for the observed modulated photocurrent. However, in practice the two types of carriers will interact with different defect levels at the same time. We have shown [10] that the main contribution to the modulated photocurrent comes from the type of carriers interacting with the level characterized by the lower $NC/\mu$ value.

For the study of 6H-SiC:V crystals two different set-ups were used. In both set-ups the sample was put onto the cold finger of dynamically pumped cryostats. In one set-up the UV excitation was provided from a set of nine light-emitting diodes (LEDs) with a peak wavelength of 385 nm (3.22 eV). The flux of these LEDs was modulated from 12 Hz to 40 kHz and the temperature varied in 5 or 10 K steps from 120 to 450 K, the maximum temperature at which the cryostat can operate. In another set-up the UV excitation was issued from a xenon lamp filtered by an interferential filter at 380 nm and chopped between 20 Hz and 2.6 kHz before impinging the sample. The temperature was varied from 130 to 740 K in 5 or 10 K steps. For both systems the background (dc) photon flux was of the order of $10^{14}$ cm$^{-2}$ s$^{-1}$ and the alternating flux was of the order of $3 \times 10^{13}$ cm$^{-2}$ s$^{-1}$.

## 3. Experimental results

### *3.1. Samples*

The samples used in this work were prepared from commercially available wafers with a thickness of $\sim$390 $\mu$m, cut out perpendicularly to the $c$ axis ($\langle 0001 \rangle$ direction) from vanadium-doped crystals of semi-insulating 6H-SiC grown by the physical vapour transport method. The (0001) Si-face surface of the wafers was polished according to the requirements for epitaxial substrates and the backside was of optical quality. Pieces of material with dimensions of $10 \times 10$ mm$^2$ were cut from the central parts of the wafers.

For the PITS and MPC measurements, arrays of two co-planar ohmic contacts ($2.1 \times 2.1$ mm$^2$) were made by evaporating a 20 nm layer of Cr and a 300 nm layer of Au on the front surface (Si-face) of the wafers followed by annealing at 500 °C. The width of the gap between the two co-planar contacts was 0.7 mm. The resistivity at room temperature of the semi-insulating 6H–SiC:V samples was $\sim 1 \times 10^{10}$ $\Omega$ cm. In the temperature range of 600–750 K, the activation energy of dark conductivity was 1.26 eV.

### *3.2. PITS results*

The aim of this paper is not to give a detailed presentation of all experimental PITS results obtained on all the 6H-SiC crystals, results that have already been released in other publications [12, 13]. Rather, we will focus significant results in order to compare with MPC results and to gain more insight into the defect distributions from this comparison.

As shown by Pawlowski *et al* [7], the visualization of a particular defect is helped by three-dimensional plots, one axis corresponding to the explored range of temperature, another axis to the range of emission rates and a vertical axis displaying the PITS function amplitude. A projection of such curves on the plane ($T$, $e_n$) with different colours for the PITS function amplitude leads to an array of spectral fringes representative of the experimental results as shown in figure 1.

In figure 1(a) two spectral fringes corresponding to two different levels were detected from the determination of the $e_n$ values at the extrema of the PITS amplitude at different temperatures ($e_{max}$), as detailed in section 2.1. These fringes were obtained from the photocurrent transients recorded with a flux equal to $10^{18}$ cm$^{-2}$ s$^{-1}$ and a pulse width pw = 50 ms. It has to be underlined that one of these fringes, observed in the upper left corner of figure 1(a), is associated with a negative amplitude of the PITS function caused by the negative amplitude of the photocurrent relaxation waveforms at short time. By means of an Arrhenius plot of $T^2/e_{max}$ as mentioned above, the activation energy of this level was found equal to $E_a = 115 \pm 5$ meV with $A = \gamma_n \sigma_n = 3.1 \times 10^2$ s$^{-1}$ K$^2$. For the second level, the parameters were found equal to $E_a = 200 \pm 10$ meV and $A = 1.5 \times 10^3$ s$^{-1}$ K$^2$.

In figure 1(b) we show PITS results obtained in almost the same temperature and emission rate range as in figure 1(a) but with a flux of $10^{17}$ cm$^{-2}$ s$^{-1}$ and a UV pulse width of 5 ms. In figure 1(b) a curved line indicates the evolution of the position of a maximum of the PITS amplitude with $T$ and $e_n$. The activation energy and $A$ coefficient of the corresponding level were found equal to $E_a = 280 \pm 10$ meV and $A = 3.0 \times 10^5$ s$^{-1}$ K$^2$, respectively.

As already mentioned, in both PITS and MPC techniques, it is impossible to know which type of carrier is responsible for the observed response. Besides, there is not much of a difference between mobilities and equivalent densities of states for free electrons and holes. Indeed, for the conduction band one has $N_{eq} = N_c = 8.9 \times 10^{19}$ cm$^{-3}$, and for the valence band $N_{eq} = N_v = 2.5 \times 10^{19}$ cm$^{-3}$ at 300 K [14]. The free carrier mobilities are of the order of $\mu_n = 400$ cm$^2$ V$^{-1}$ s$^{-1}$ and $\mu_p = 100$ cm$^2$ V$^{-1}$ s$^{-1}$ for electrons and holes, respectively [15]. Hence, in the dark and with the Fermi level in the middle of the gap one would have a contribution of free electrons to the current approximately 10 times higher than the free hole contribution ($8.9/2.5 \times 400/100$). But this factor of ten can be easily compensated if the Fermi level is slightly shifted towards the valence band. Besides, under illumination the free hole and free electron densities largely depend on the defect densities present in the gap.

A tentative identification of the levels shown in figures 1(a) and (b) was made by the comparison of the activation energies $E_a$ and $A$ coefficients obtained in PITS with those obtained from DLTS or admittance spectroscopy. The shallower level ($E_a = 115$ meV) was attributed to nitrogen impurities [14, 16] that introduce a donor level close to the conduction band, and the deeper level ($E_a = 280$ meV), observed with a lower photon flux, was linked to boron impurities that introduce an acceptor level close to the valence band [14, 17]. The centre with intermediate activation energy ($E_a = 200$ meV) is likely to be attributed to aluminium impurities giving an acceptor level close to the valence band [14, 18].

We have concentrated on these three levels because they raise the following questions: (i) how is it possible in the same temperature range to observe both an electron trapping level (nitrogen) and a hole trapping level (aluminium); (ii) what is the origin of the negative PITS amplitude linked to the nitrogen level; and (iii) why, by decreasing the flux and pulse width, are the levels related to N and Al not detected whereas a new hole trapping level related to boron exhibits a major contribution to the PITS signal in the same temperature range? To provide an answer to these questions, we shall use a numerical simulation presented in section 4.

### *3.3. MPC results*

The r-DOS measured by MPC on a sample of 6H-SiC:V crystal are presented in figure 2. This quantity depends only on experimental parameters. However, if the absolute value of the r-DOS can be known, it is more difficult to scale its variation with the energy, since the energy scaling depends on the choice of the attempt-to-escape frequency (see equation (7)). In figure 2 we have taken arbitrarily $\nu = 10^{12}$ s$^{-1}$ to give an overview of the r-DOS versus energy. It is clear that for each defect level, revealed by a peak in the r-DOS spectra, the $\nu$ may be different depending on its capture cross section. A method to determine the proper $\nu$ for a given peak has been explained elsewhere [4].

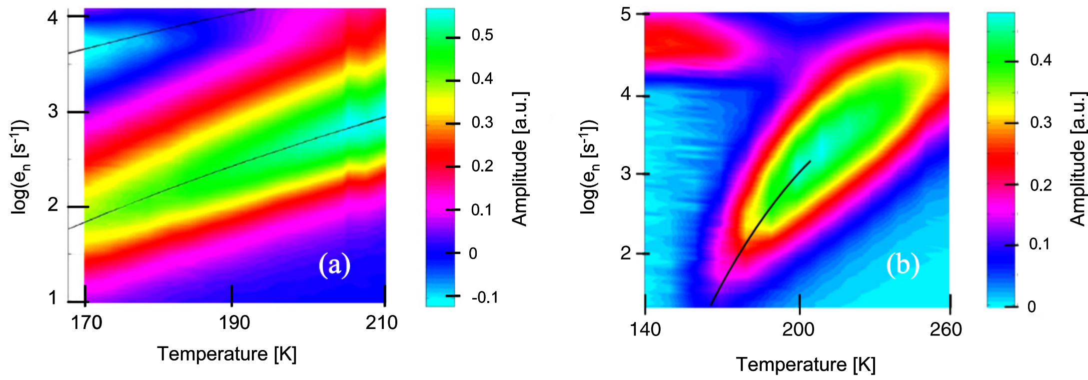


**Figure 1.** (a) Experimental PITS fringes obtained in the temperature range 170 K $\leqslant T \leqslant$ 210 K for a flux of $10^{18}$ cm$^{-2}$ s$^{-1}$ and a pulse width of 50 ms. Full lines indicate the temperature dependences of $e_{max}$ for two detected defect centres. Note that the PITS amplitude corresponding to the defect level with the higher emission rate shown in the upper left corner is negative. (b) Experimental PITS fringe obtained in the temperature range 140–260 K for a flux of $10^{17}$ cm$^{-2}$ s$^{-1}$ and a UV pulse width of 5 ms. The full line indicates the temperature dependence of $e_{max}$ for a defect centre.

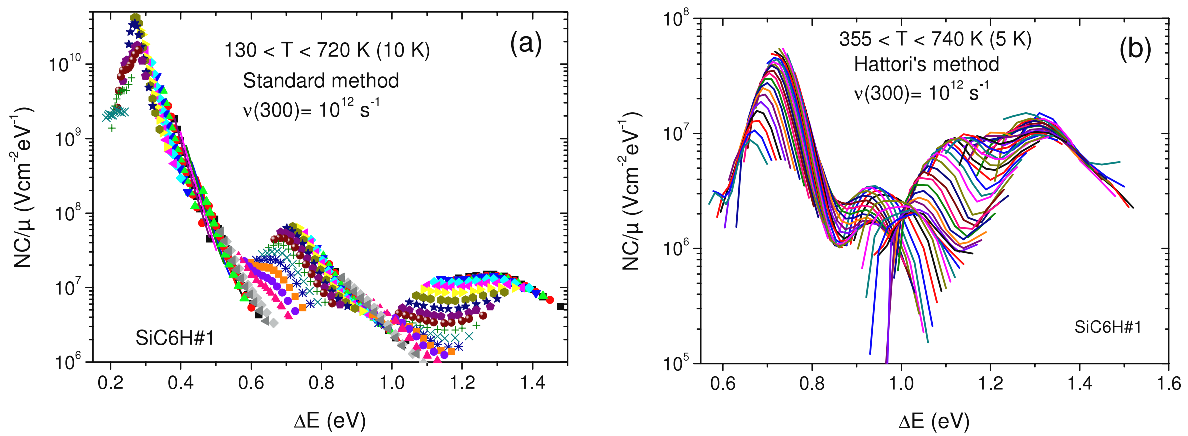


**Figure 2.** Reduced density of states spectra obtained by MPC applied to a sample of 6H-SiC:V crystal. (a) Peaks revealed in the whole temperature range. (b) Zoom on the density of states for the deep defect levels probed at high temperatures.

We would like to recall shortly that the r-DOS determined from MPC data, and in particular those in figure 2, are made of a collection of data obtained at several temperatures and frequencies of the modulated photon flux. In figure 2(a) each temperature corresponds to a set of symbols and each symbol within a given set corresponds to a frequency of the modulated flux. In figure 2(b) symbols have been replaced by lines giving a clearer picture than symbols. In both figures the 'true' r-DOS is given by the upper envelope of the curves [10]. In figure 2(a) measurements were done each 10 K and in figure 2(b) measurements were done each 5 K. The method used to extract the r-DOS is not the same in figures 2(a) and (b). In figure 2(a) we have used the 'standard' method, i.e. equation (5) [9], and in figure 2(b) we have used the method proposed by Hattori *et al* [11]. Hattori's method allows one to obtain narrower peaks of r-DOS but it is based on the derivative of an experimentally measured quantity and could be very noisy, especially when the measured photocurrent is low. As was the case here at low temperature, we preferred to give an overview of the r-DOS with the 'standard' method to show the very huge peak that appears close to one band edge.

### 3.4. Discussion

The main levels detected by the PITS experiment are presented in table 1. It can be seen that the same impurity is at the origin of different defect levels depending on the configuration in which it is included in the material. The sites to be considered are either in an hexagonal (hex.) configuration or in two different cubic configurations ($k_1$ and $k_2$) of the SiC lattice and it is clear that the surroundings of an impurity play a role on the gap position of the corresponding energy level [19].

The defect levels found by the MPC method are also displayed in table 1, and a tentative correlation with the PITS data is shown. We have converted the $A$ values found from PITS into $\nu$ values, to be compared with the $\nu$ values found in the MPC experiment. For this purpose we have calculated the attempt-to-escape frequency at 300 K, $\nu(300)$ using the relation between $A$ and the emission rate $e$ for a defect level

**Table 1.** Electronic properties of some defects determined by PITS or MPC and introduced in the numerical simulation. The electron (hole) traps are labelled with e (h).

| Tentative identification of the traps | $E_{PITS}$ (meV) | $A$ ($s^{-1}$ $K^{-2}$) | $\nu_{PITS}(300)$ ($s^{-1}$) | $E_{MPC}$ (meV) | $\nu_{MPC}(300)$ ($s^{-1}$) |
|---|---|---|---|---|---|
| N related (e trap) | $180 \pm 10$ | $1.5 \times 10^4$ | $1.4 \times 10^9$ | | |
| $N_C$ at $k_1$ site (e trap) | $115 \pm 5$ | $3.1 \times 10^2$ | $2.8 \times 10^7$ | | |
| $B_{Si}$ in hex. site (h trap) | $280 \pm 10$ | $3.0 \times 10^5$ | $2.7 \times 10^{10}$ | 230–250 | $\sim 2.5 \times 10^{11}$ |
| $Al_{Si}$ in hex. site, (h trap) | $200 \pm 10$ | $1.5 \times 10^3$ | $1.4 \times 10^8$ | | |
| $V^{3+/4+}$ cubic site, (e trap) | $780 \pm 20$ | $(1.3–9.0) \times 10^7$ | $(1.2–8.1) \times 10^{12}$ | 700–740 | $\sim 2.0 \times 10^{12}$ |
| $V^{3+/4+}$ hex. site, (e trap) | $870 \pm 20$ | $(3.0–30) \times 10^6$ | $(2.7–27) \times 10^{11}$ | 860–900 | $\sim 2.5 \times 10^{11}$ |
| UD1 line, (e trap) | 1000 | $3.7 \times 10^6$ | $3.3 \times 10^{11}$ | | |
| V related (e trap) | $1250 \pm 30$ | $5.0 \times 10^8$ | $4.5 \times 10^{13}$ | 1200–1250 | $\sim 2.5 \times 10^{11}$ |
| $V^{5+/4+}$ (h trap) | $1360 \pm 40$ | $2.4 \times 10^8$ | $2.2 \times 10^{13}$ | | |

located at $\Delta E$ from one band or the other:

$$e = AT^2 \exp\left(-\frac{\Delta E}{k_b T}\right) = C(300) N_{eq}(300) \left(\frac{T}{300}\right)^2 \exp\left(-\frac{\Delta E}{k_b T}\right), \quad (8)$$

where $C(300)$ is the capture coefficient and $N_{eq}(300)$ is the equivalent density of states at the band edge at 300 K. This leads to $\nu(300) = A \times 300^2$ $s^{-1}$. The definition of $\nu(300)$ does not depend on the considered type of carrier and the values can be directly compared from one experiment to the other.

It can be seen in table 1 that activation energies and attempt-to-escape frequencies of some levels are put into evidence by both techniques with rather good agreements. For instance, the $V^{3+}/V^{4+}$ centres, both in cubic and hexagonal sites, are detected by each technique with the same energy positions and attempt-to-escape frequencies of the same order of magnitude. Though the agreement is not perfect concerning the $\nu$ values, we must underline that in the PITS technique they come from an extrapolation of the Arrhenius plot towards $T = 0$ K, and, in the MPC experiment, from the adjustment of the energy scale where $\nu$ is included in a logarithmic expression (see equation (7)). Hence, the $\nu$ values given in table 1 are subject to errors and we estimate that they are obtained within a factor of 5.

Considering the equivalence in the results obtained by both techniques, shown in table 1, some discrepancies can be underlined. Firstly, depending on the method, two very different attempt-to-escape frequencies (by a factor of a hundred) are found for the level located around 1.2 eV (vanadium-related). It may be the two techniques are sensitive to two different levels located at the same energy simply because the experimental conditions are not the same, the fluxes being very different. Secondly, the MPC technique seems to probe levels exchanging electrons with the conduction band except that we do not detect the N level. Besides, using the MPC we detect a level at $\sim 0.24$ eV that we could attribute to boron. However, boron is a 'hole' trap and it seems strange that MPC probes the boron states and not the aluminium level which is shallower than the boron level. On the other hand, the level at 0.24 eV could be attributed to oxygen [20], an 'electron' trap, but this raises the question of why oxygen is not seen with the PITS technique? These last issues will find an explanation by means of the numerical simulation we have developed.

## 4. Simulation

A numerical simulation was developed to understand the basic mechanisms of carrier trapping, emission and recombination occurring in the MPC and PITS experiments [21]. In this simulation one can introduce transport parameters, such as the bandgap, free carrier mobilities and equivalent densities of states at the band edges, as well as the defect level properties like density of states, energy position and capture coefficients. To achieve the numerical simulation the bandgap is divided into 500 discrete energy steps. Densities of defect states were introduced as Gaussian distributions with a standard deviation of 5 meV. For the MPC we calculate the modulus and phase shift of the alternative photocurrent by solving the general equations giving the free carrier concentrations (for these equations see [10]). The PITS photocurrent is calculated by solving the continuity equations by means of an Euler implicit method. This method allows a fast calculation of the evolution of the photocurrent transient from the onset of the excitation up to 10 s after the end of it.

We have limited our simulation to the study of the 'main' traps, i.e. those whose contribution to the PITS current was found to be predominant in the vast majority of samples. So, the introduced levels were those related to nitrogen, boron, aluminium and vanadium in the cubic site and the UD1 centre. We shall see that an 'extra' level, attributed to oxygen, must also be taken into account to explain the MPC results. The main difficulty in performing such numerical simulations is that to characterize each defect centre one needs five parameters: maximum value $N_{max}$ and standard deviation of the Gaussian energy distribution of states, from which the centre concentration can be calculated, energy position of the maximum and capture coefficients for electrons and holes. Therefore, if one wants to reproduce the experimental behaviour taking into account the major defect levels detected by both experiments (say, six different centres) one has to deal with thirty adjustable parameters.

However, since we only want to provide a better understanding of the experimental results and to reveal the general mechanisms, we can precisely use these results to decrease the number of adjustable parameters. In the simulation, for each distribution of states corresponding to a defect centre, we have an experimental estimate of the energy position of the maximum as well as a good estimate of at least one of the capture coefficients. To define rather narrow levels

in the bandgap, we have chosen a standard deviation of 5 meV for any Gaussian distribution related to a defect centre. Hence, the number of adjustable parameters drops to twelve. This last number is still high but we have also some constraints to follow in order to reproduce experimental results that will provide guidelines and limit the possibilities of variation of these adjustable parameters.

First of all, the simulation must reproduce the results in a temperature range from 100 to 700 K with the use of three different values of the photon flux, $10^{18}$ and $10^{17}$ cm$^{-2}$ s$^{-1}$ for the PITS technique and $10^{14}$ cm$^{-2}$ s$^{-1}$ for the MPC.

Considering the PITS experiment, one major point must be reproduced: the 'negative' transient photoconductivity observed at low temperature taking into account that this negative transient was observed with the higher photon flux ($10^{18}$ cm$^{-2}$ s$^{-1}$) and not with the lower one ($10^{17}$ cm$^{-2}$ s$^{-1}$). Besides, depending on the photon flux used and pulse width, different centres—Al, B and N—were detected in the same temperature range, Al and B being hole traps and N being an electron trap. Moreover, Al and N levels were detected with a pulse width of pw $\approx$ 50 ms and a photon flux of $10^{18}$ cm$^{-2}$ s$^{-1}$, whereas the B level was detected with pw $\approx$ 5 ms and a photon flux of $10^{17}$ cm$^{-2}$ s$^{-1}$.

Considering the MPC experiment, the numerical simulations must reproduce the very high peak observed at low temperature (i.e. low energy range). There must be a factor of around one thousand between the shallower peak height and the deeper ones.

We have first studied the dependence of the simulated PITS transients on the defect centre parameters. First, we have introduced the following parameters characteristic of 6H-SiC: for the conduction band we have chosen $N_c = 8.9 \times 10^{19}$ cm$^{-3}$ and for the valence band $N_v = 2.5 \times 10^{19}$ cm$^{-3}$ at 300 K [14]. These quantities were assumed to vary with temperature as $T^{1.5}$. The bandgap for 6H-SiC was taken at $E_g = 3$ eV and was varied with a temperature coefficient of $-0.08$ meV K$^{-1}$ [22].

The capture coefficients of some centres can be deduced from the $A$ or $\nu(300)$ experimental values. Using the equivalent densities of states, we have the following relations: $C_n \approx A \times 10^{-15}$ and $C_p \approx A \times 3.6 \times 10^{-15}$ cm$^3$ s$^{-1}$ from which capture coefficients were obtained using the data given in table 1.

Other parameters, corresponding to experimental conditions, such as for example the photon flux impinging the sample, the excitation pulse width or the temperatures at which the experiment was performed, can be introduced in the simulation.

The best way to introduce the defect levels in the numerical calculation is to start with the deeper ones because they influence the results over the whole range of temperatures. At high temperature the splitting of the quasi-Fermi levels is small, and only the deepest states will see their occupancy modified. Therefore, they are the only levels that are likely to be seen if one also takes into account that the carrier emission from these deep levels is activated with $T$. At low temperature, they will play the role of recombination centres and will have an important influence on the free carrier density. That is why we have introduced first a defect level related to vanadium and another one responsible for the UD1 centre observed experimentally [13]. These two defects have different electronic properties. The vanadium is a multivalent centre. Indeed, experimentally one observes either the $V^{3+}/V^{4+}$ transition (negatively charged/neutral) by emission of an electron or the $V^{5+}/V^{4+}$ transition (positively charged/ neutral) by emission of a hole. According to the data presented in table 1, the respective energy levels of these transitions were fixed at 0.77 eV below the conduction band edge $E_c$ (i.e. 2.23 eV above the valence band edge $E_v$) and 1.32 eV above the valence band, respectively. Therefore, vanadium was considered as an amphoteric centre having $-/0/+$ charge states with a correlation energy $E_{corr} = 0.91$ eV. This correlation energy is the excess energy to provide to an electron to transform a neutral $V^{4+}$ centre that already contains one electron, into a negative $V^{3+}$ centre that contains two electrons. Of course the statistics of occupancy of such a defect differs from the 'usual' Fermi–Dirac statistics since one has to define occupation functions for each state of charge. The evolution of these occupation functions under illumination was studied in a previous paper and we shall not come back to this topic (see, for instance, [23] and references therein). The electron and hole capture coefficients were fixed according to the experimental data. Table 2 summarizes the experimental parameters used in the simulation and gives indications of the parameters to be determined, for the six different centres we have considered.

Set alone in the bandgap, the vanadium centre fixes the Fermi level around 1.23 eV below the conduction band. To fix the Fermi level in the middle of the bandgap, around 1.5 eV, the level corresponding to the UD1 centre was assumed to be a monovalent acceptor level (neutral if empty, negatively charged if filled) and set at 2 eV above $E_v$ with a concentration of the same order as the vanadium. However, we shall see in the following that the position of the Fermi level is probably more dependent on the shallow levels (Al or N) concentrations than on the deep level concentration. Hence, we might have chosen a donor state for the UD1 level but it would not have had a large influence on the final results.

These two centres, V and UD1, have been introduced in the simulation with a concentration of $4 \times 10^{15}$ cm$^{-3}$ at the energy positions given by experimental results. The hole and electron capture coefficients for the V centre and the electron capture cross section for the UD1 centre were also fixed from the experimental data. Two different simulations were performed: first, varying the capture coefficient for holes of the UD1 centre, $C_p$ (UD1), maintaining the same concentrations for each centre and, second, varying the concentration of the UD1 centre keeping $C_p$ (UD1) constant.

We have found that the contribution of the emission of electrons from the $V^{3+}$ to the photocurrent was decreasing with decreasing $C_p$ (UD1). This behaviour can be explained by the fact that a decrease of $C_p$ (UD1) lowers the recombination via this level because less holes are captured. Hence, the capture of holes, to fulfil the recombination process, takes place essentially via the V centre. The increased capture of holes reduces the $V^{3+}$ concentration and its contribution to the photocurrent by the emission of electrons. According to

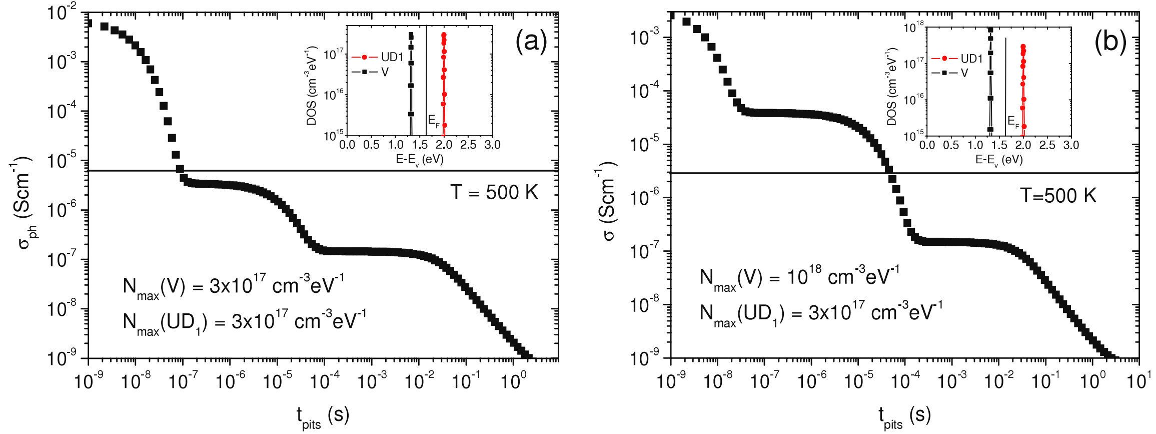


**Figure 3.** Effect of density of states on the time evolution of the simulated photoconductivity relaxation in the PITS experiment at a temperature of 500 K after switching off the UV pulse. (a) The maximum densities of states of the vanadium and UD1 centres were both taken equal to $3 \times 10^{17}$ cm$^{-3}$ eV$^{-1}$. (b) The maximum of the V density was increased up to $10^{18}$ cm$^{-3}$ eV$^{-1}$. In each figure the insert displays the density of states (DOS) introduced in the simulation. The dark Fermi level position is indicated by a vertical line.

**Table 2.** Parameters coming from the experimental results shown in table 1 for six defect centres in 6H-SiC introduced in the simulation. The cells for missing values to be found are marked with a '—'.

| Defect | V | UD1 level | Al | N | B | O |
|---|---|---|---|---|---|---|
| $E - E_v$ (eV) | **1.32** | **2.0** | **0.2** | **2.86** | **0.30** | **2.75** |
| $E_{corr}$ (eV) | **0.91** | | | | | |
| $N_{max}$ (cm$^{-3}$ eV$^{-1}$) | — | — | — | — | — | — |
| Concent. (cm$^{-3}$) | — | — | — | — | — | — |
| $C_n$ (cm$^3$ s$^{-1}$) | **$4.0 \times 10^{-8}$** | **$4.0 \times 10^{-9}$** | — | **$2.0 \times 10^{-13}$** | — | **$5.0 \times 10^{-8}$** |
| $C_p$ (cm$^3$ s$^{-1}$) | **$9.0 \times 10^{-7}$** | — | **$4.5 \times 10^{-12}$** | — | **$1.1 \times 10^{-9}$** | — |

the simulation we have estimated that the $V^{3+}$ influence on the PITS transient could not be detected experimentally for $C_p$ (UD1) $< 10^{-8}$ cm$^3$ s$^{-1}$.

Keeping $C_p(\text{UD1}) = 10^{-8}$ cm$^3$ s$^{-1}$ it was found that an increase of the UD1 centre concentration by a factor of ten suppressed almost completely the $V^{3+}$ influence, whereas a decrease by the same factor enhanced it. The reason of this result is not a modification of the recombination path as in the previous case. In this case one would expect exactly the reverse behaviour. The different $V^{3+}$ influence is due to the modification of electrical neutrality. When the UV pulse is shone onto the sample, the filling of the UD1 centre by electrons creates a negative charge (acceptor level). If the UD1 level concentration is high this negative charge prevents the filling of the $V^{3+}$ level since it is enough to equilibrate the positive charge created elsewhere, for instance by the $V^{5+}$ states. Since the $V^{3+}$ level is not filled it cannot contribute to the transient photocurrent once the UV pulse is turned off.

We have also performed some tests on the influence of the vanadium concentration on the PITS signal. Taking into account the dynamic of the amplifier used in the PITS measurements and the signal-to-noise ratio, we have estimated that to be properly detected the ratio between the signal before and the signal after the UV pulse is turned off could not be higher than a factor of one thousand. We present in figure 3(a) the simulated time evolution of the photoconductivity relaxation in the PITS experiment when the maximum densities of states for V and UD1 defects are both taken equal to $3 \times 10^{17}$ cm$^{-3}$ eV$^{-1}$. The first decrease is due to recombination and trapping of free carriers. The rate of decrease is slowed down when electrons are emitted from the $V^{3+}$ level (first plateau). When all the electrons are emitted from the $V^{3+}$ level recombination resumes and is slowed down again when electrons are emitted from the UD1 centre (second plateau). Subsequently, recombination resumes and the photoconductivity tends towards zero (conductivity tends towards the dark conductivity value). The horizontal line is set at a level a thousand times lower than the maximum value of the transient photoconductivity. Clearly, taking account of the experimental limitations, neither the $V^{3+}$ nor the UD1 centre could be detected since their contributions are well below the line. In figure 3(b) we present the same evolution but in the numerical simulation the maximum density of the V centre was taken equal to $10^{18}$ cm$^{-3}$ eV$^{-1}$. The contribution of the emission of electrons from the $V^{3+}$ level to the photoconductivity is well above the line and the $V^{3+}$ level should be detected at the temperature at which the simulation was performed as was the case experimentally [12, 13]. Hence, the results of the numerical simulation suggest that the vanadium concentration must be higher than $4 \times 10^{15}$ cm$^{-3}$ to be detectable. A vanadium concentration of $1.3 \times 10^{16}$ cm$^{-3}$ as in figure 3(b) would agree with experimental results.

The 'negative' photoconductivity phenomenon has been well known for a long time [24]. In our samples we observed a fast decrease of the current after the UV pulse was turned off followed by a rapid rise and then a slow decrease at very

long times. This phenomenon could be taken as negative photoconductivity depending on the mean baseline. Indeed, if the UV pulse repetition rate is high, these down and up variations can appear as a spike below the mean baseline of the current transient. For this reason we will still continue to call it negative photoconductivity (NPC) though the experimental baseline may be higher than the steady-state dark current.

We can explain the NPC phenomenon considering the case of the electrons as an example. After the UV pulse is switched off, trapping and recombination of the excess of free carriers gives rise to the observed fast decrease of the photocurrent. If the defect levels configuration is such that the electron lifetime increases, and at the same time a shallow level releases electrons towards the conduction band, then a rise of the measured current is observed due to the increase of the free electron density. This increase is subsequently followed by a decrease of the current as the recombination goes on. An increase of the electron lifetime is due to a saturation of the deep levels by the same type of carriers so the electron capture rate tends towards zero. This saturation means that, during a non-negligible time range, there are no holes left for the electron to recombine with.

To reproduce this behaviour we have introduced two shallow levels corresponding, respectively, to aluminium and nitrogen at the energy positions and with capture coefficients, for holes and electrons, respectively, determined from the experimental results. The unknown parameters like $C_n$ for Al and $C_p$ for N were at first taken to be very low and we have studied the influence of Al and N concentrations on the occurrence of the NPC. Besides, at this point of the paper we have chosen rather high values for the N and Al concentrations to underline their influence on the transient current. These values will be adjusted later to match experimental data.

To reproduce the NPC we have found that the concentrations of Al and N should be higher than the V concentration. In that case the reader must note that from neutrality considerations the Al and N concentrations should be almost equal to maintain the dark Fermi level position close to midgap. Taking account of the Al and N energy positions in the bandgap and of their respective hole and electron capture coefficients, nitrogen releases electrons toward the conduction band before Al releases holes toward the valence band after the UV pulse is switched off. These electrons are trapped in the deep states, formed by V and UD1 centres, where they recombine with the holes set in these levels by the illumination. If the number of released electrons is low, there are enough holes on the deep levels to fulfil recombination. Besides, when holes are released slightly later from the Al level, they will also be captured by the deep states and will enhance the recombination process. It is therefore impossible to observe the NPC because the electron concentration in the conduction band is systematically decreasing. On the other hand, the higher the N concentration the higher the number of electrons emitted to the conduction band. With a nitrogen concentration larger than the deep centre concentrations, the emitted electrons eventually saturate the deep levels and the electron lifetime increases. Such a behaviour linked to a change in the recombination process related to the presence of different types of defect states is somewhat similar to the sensitization process where a thermal quenching of steady-state photoconductivity can be observed [25]. However, in our case, changes in the recombination process are observed in the time domain rather than in the temperature dependence of the steady-state response. If electrons are still emitted from nitrogen atoms after the saturation of the deep states, the free-electron concentration increases and the NPC is then clearly visible. Subsequently, the release of holes from the Al level will provide the opposite type of charge carriers for the recombination to resume. In that case the thermal emission of holes from the Al level is observed via the recombination of the electrons of the conduction band. This also explains why the Al level close to the valence band can be seen experimentally, even though electrons are the majority carriers: the electron lifetime and recombination are controlled by the thermal emission of holes from the Al level.

This is illustrated in figure 4(a) where the simulated time evolution of the free-electron (n) and hole (p) concentrations are depicted after the UV pulse is turned off. The simulation was performed with the parameters displayed in table 2, at a temperature of 175 K with rather high values of the Al and N concentrations: $[\mathrm{Al}] = [\mathrm{N}] = 4 \times 10^{18}$ cm$^{-3}$. The NPC is clearly visible from short times up to $t \approx 300$ $\mu$s. The concentration of free holes is also clearly negligible compared to that of electrons such that it would be impossible to detect experimentally their contribution even when the excess electron concentration falls towards zero by recombination. However, if one vertically shifts the free-hole concentration curve to adjust it to that of free electrons for $t > 300$ $\mu$s (see the full line in figures 4(a) and (b)), it clearly appears that both evolutions are strictly the same from 300 $\mu$s up to $t = 0.03$ s. This is due to the control of electron recombination by the emission of holes from the Al level: the free-electron concentration follows exactly the emission of holes from the Al level. When the electron concentration falls below $10^8$ cm$^{-3}$, for $t > 0.1$ s, a kink—indicated by the vertical arrow in figure 4(a)—appears on the curve representing the hole concentration evolution that corresponds to a sudden increase of the free-hole lifetime, since there is only a small concentration of free electrons left for the recombination of holes.

The next point we have studied is the influence on the NPC of the electron and hole capture coefficients, $C_n$ (Al) and $C_p$ (N), for the aluminium and nitrogen centres, respectively. We have found that these coefficients cannot be too high. Indeed, just after the UV pulse is turned off, all the levels are filled and act as recombination centres. If $C_n$ (Al) is chosen too high, the electrons released from the N level recombine also via the Al level. The addition of this recombination path to the path involving the deep states suppresses the NPC, because the electrons emitted for the N level recombine too rapidly and no increase of the free-electron concentration can be achieved. If $C_p$ (N) is chosen too high, the filling of N is limited during the illumination because the high capture of holes by this centre lowers the number of trapped electrons. So, the filling of the N centre with electrons decreases with increasing $C_p$ (N) and the NPC disappears because there are not enough electrons

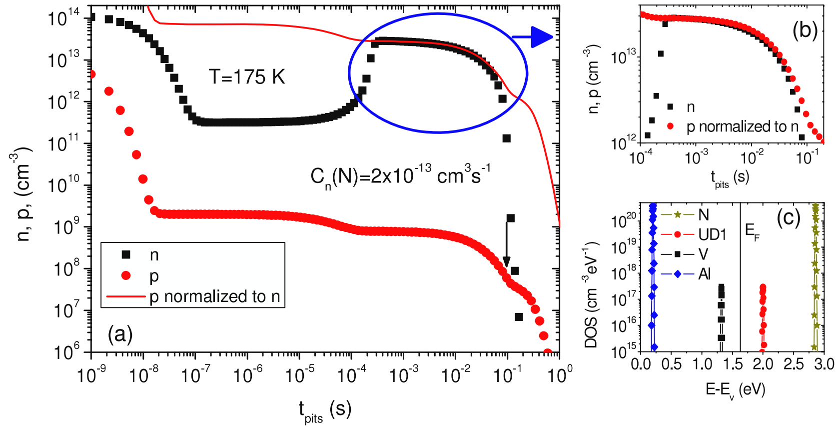


**Figure 4.** (a) Time evolution of the free-electron (n) and hole (p) concentrations simulated at $T = 175$ K with the level parameters displayed in table 2. (b) p($t$) concentration adjusted to n($t$) concentration showing that both concentrations follow the same time dependence over two decades of time after the end of the NPC. (c) The density of states (DOS) introduced in the simulation. The dark Fermi level position $E_F$ is indicated by a vertical line.

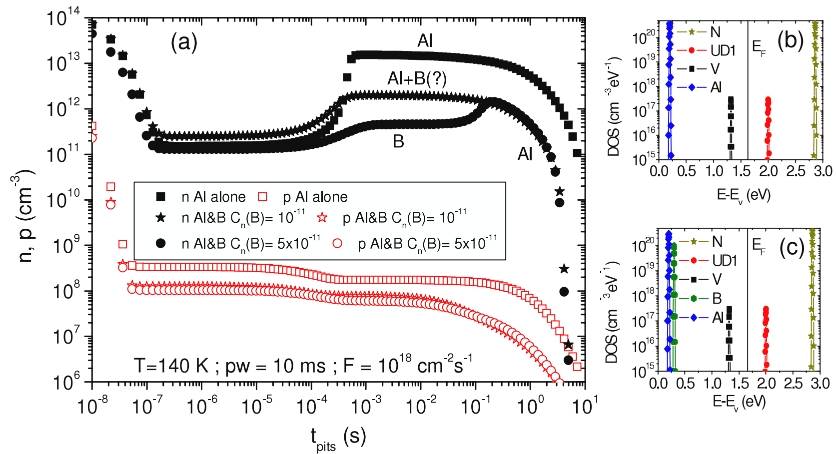


**Figure 5.** (a) Influence of the boron level on the time evolution of the free-electron (n) and hole (p) concentrations. The numerical simulations were performed at 140 K. For $t > 10^{-3}$ s the Al and B labels indicate which defect centre controls the recombination. (b) and (c) show the density of states used for the calculations: (b) without boron and (c) with boron. A vertical line in (b) and (c) indicates the position of the dark Fermi level.

emitted from the N level to saturate the deep states and to increase the free-electron concentration after the UV pulse is turned off. However, the ranges of values for $C_n$ (Al) and $C_p$ (N) for which NPC can be reproduced are rather large, say $C_n(\text{Al}) < 10^{-9}$ cm$^3$ s$^{-1}$ and $C_p(\text{N}) < 10^{-7}$ cm$^3$ s$^{-1}$. It is worth emphasizing that precise values of these coefficients cannot be determined by means of numerical calculations and only these upper limits can be proposed.

Next, we have introduced the boron level. Following the experimental results (see table 2), the energy position was fixed at 0.3 eV above the valence band and the hole capture coefficient taken equal to $C_p(\text{B}) = 1.1 \times 10^{-9}$ cm$^3$ s$^{-1}$. The maximum density of states was taken equal to $N_{max}(\text{B}) = 10^{20}$ cm$^{-3}$ eV$^{-1}$. The choice of this rather high value of $N_{max}(\text{B})$ was determined by the experimental results showing that at a high flux, of the order of $10^{18}$ cm$^{-2}$ s$^{-1}$, the negative photoconductivity linked to the N level is visible simultaneously with the thermal emission of holes from the Al level. On the other hand, with a lower flux, for instance $10^{17}$ cm$^{-2}$ s$^{-1}$, only the boron level is visible. Intuitively, it means that, at high flux, the Al and B levels are filled but it is the Al level that is mainly observed by the emission of holes controlling the recombination of electrons emitted from the nitrogen level, whereas at lower flux, the B level is the main level filled, because the quasi-Fermi level splitting is smaller, and it is the boron level that controls the recombination of the electrons emitted from the N level.

The influence of the boron level can be highlighted by the study of the influence of its capture coefficient for electrons $C_n(\text{B})$ and of the influence of the UV pulse width on the free-carrier concentrations. The time evolutions of the free-electron and hole concentrations showing the influence of the boron level on the photocurrent relaxation waveform are displayed in figure 5(a). To calculate these evolutions, the flux was fixed at $10^{18}$ cm$^{-2}$ s$^{-1}$ and the pulse width at 10 ms. In a first calculation, only the Al level was introduced in the simulation (full squares). The NPC is clearly visible with a minimum for the n concentration between $t = 10^{-7}$ and $10^{-4}$ s. In

this range of time, recombination is mainly controlled by the deep states (V and UD1). When these levels are neutralized by the electrons emitted from the N level, the free-electron concentration increases. Then the recombination is controlled by the emission of holes from the Al level: the time evolutions of free-electron and hole concentrations (full and open squares, respectively) are parallel over a few decades of time. In a second calculation, the boron level was added with an electron capture coefficient $C_n(B) = 10^{-11}$ cm$^3$ s$^{-1}$ (full stars). The time range of the NPC is the same since it is fixed by the electron emission from the N level and saturation of the deep states. However, it is hard to say which centre, Al or B, controls the recombination process between $t = 10^{-3}$ and $10^{-1}$ s, after the end of the NPC phenomenon. Indeed, either B or Al centres can play a role in this recombination process in this time range, hence the question mark in figure 5(a). In a third calculation, $C_n(B)$ was increased up to $5 \times 10^{-11}$ cm$^3$ s$^{-1}$. It can be seen in figure 5(a) (full circles) that a second plateau appears for $10^{-3}$ s $< t < 10^{-1}$ s, as if the NPC was observed up to $t \approx 10^{-1}$ s and could result from two independent processes. For $t$ lower than $5 \times 10^{-4}$ s the recombination is controlled by the deep states and that is why the n concentration is the same as in the case without boron. Between $10^{-4}$ and $10^{-3}$ s, the n concentration increases because the deep states are saturated and electrons are still emitted from the N level towards the conduction band. Simultaneously, the $C_n(B)$ value is such that the boron level takes the control over the recombination process for $t$ between $10^{-3}$ and $10^{-1}$ s, until it is completely saturated by the electrons emitted from the N level. Then, the free-electron concentration increases again still by the electron emission from the N level but the recombination resumes with the holes emitted from the Al level. Since this 'double' NPC was not observed, it fixes a limit to the $C_n(B)$ maximum value not exceeding $10^{-11}$ cm$^3$ s$^{-1}$.

With the presence of boron, we have also studied the influence of the UV pulse width and photon flux on the variations of the free-carrier concentrations. Indeed, experimentally boron was detected at a short pulse width (pw = 5 ms) and at a low photon flux ($10^{17}$ cm$^{-2}$ s$^{-1}$), whereas aluminium was detected with pw = 50 ms and a high photon flux ($10^{18}$ cm$^{-2}$ s$^{-1}$). To explain this point, figure 6 displays the variations with time of the free-carrier concentrations calculated in simulations assuming a photon flux of $10^{18}$ cm$^{-2}$ s$^{-1}$ and a temperature of 140 K for two different pulse widths (1 and 10 ms). The value of $C_n(B)$ was chosen equal to $5 \times 10^{-11}$ cm$^3$ s$^{-1}$. For pw = 10 ms we have obtained and plotted the same curves for n and p as in figure 5(a) and the interpretation is the same. For pw = 1 ms only the boron level, located deeper from the valence band than the aluminium level, has the possibility to be filled by holes. Indeed, as the UV illumination goes on, the quasi-Fermi levels are splitting apart while equilibrium tends to be established in the sample. If the time of illumination is too short for the quasi-Fermi levels to be split enough, then only the deeper levels are filled. The differences in the filling of the boron and aluminium levels with holes for pw = 1 and 10 ms are also reflected by the differences in the free-hole concentrations, much lower for pw = 1 ms than for pw = 10 ms (see figure 6). For electrical neutrality reasons, if the aluminium level is not filled with holes, the charge of the nitrogen level will only compensate for the charge of the boron level and thus will contain fewer electrons than in the case of a long pulse width. Therefore, these electrons, when emitted, will not fully neutralize the boron level as was the case with pw = 10 ms but will recombine with the holes emitted from the boron level. The second rise of the electron concentration around $t = 0.1$ s when pw = 10 ms is not observed in the case when pw = 1 ms because the recombination of the electrons emitted from the N level is completely controlled by the holes emitted from the boron level. Consequently, when pw = 10 ms, the decrease of the n concentration at very long time ($t > 1$ s) is controlled by the Al level. On the other hand, when pw = 1 ms, it is controlled by the boron level. Moreover, with a short pulse width, this effect will be even amplified with a lower photon flux because only the deepest boron states will be filled by the pulse.

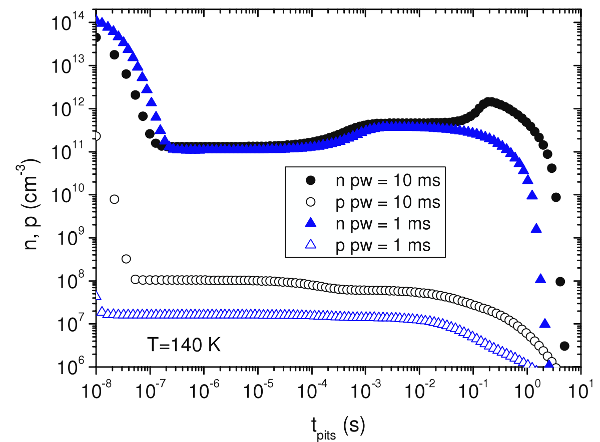


**Figure 6.** Influence of the UV pulse width (pw) on the time evolutions of the free-carrier concentrations (n and p). The photon flux was chosen equal to $10^{18}$ cm$^{-2}$ s$^{-1}$. The numerical simulation was performed at 140 K.

On the grounds of the mechanisms described above, a simple model for the density of states in 6H-SiC:V can be drawn from the results of the simulation taking into account five defect centres, namely Al, B, V, UD1 and N. The nitrogen and boron concentrations obtained in the crystals from secondary ion mass spectroscopy (SIMS) measurements were found to be of the order of $4 \times 10^{16}$ cm$^{-3}$. In the calculations, the concentrations of Al, N and B introduced in the simulations have been progressively reduced from the values exceeding $10^{18}$ cm$^{-3}$ and adjusted by checking that the experimental PITS features were still reproduced. However, to match the MPC experimental results, we had to take into account a sixth level that was attributed to oxygen [20]. The final results of the simulation matching both the PITS and MPC experimental features are shown in table 3.

Although the nitrogen and boron concentrations are slightly higher than the SIMS data, the whole picture seems to be realistic. As a matter of example, we present in figure 7 the results of the numerical simulations of the PITS experiment: with pw = 10 ms and a photon flux of

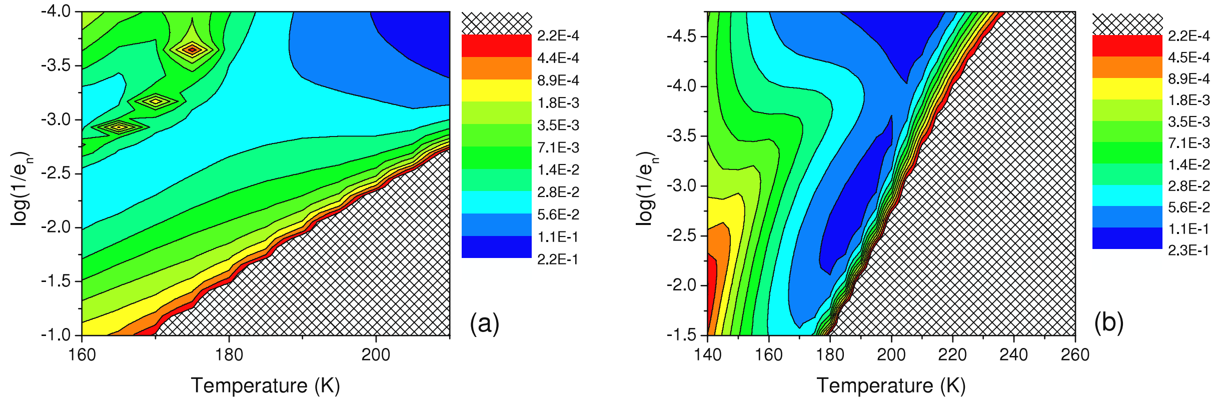


**Figure 7.** Results of the simulation of the PITS experiment with pw = 10 ms and a flux of $10^{18}$ cm$^{-2}$ s$^{-1}$ (a), and with pw = 1 ms and a flux of $10^{17}$ cm$^{-2}$ s$^{-1}$ (b). The PITS signal amplitude is indicated by different colours in arbitrary units as in figure 1.

**Table 3.** Summary of the parameters used in the simulations to reproduce both the PITS and MPC experimental results. Values in bold come from experiments.

| Defect | V | UD1 level | Al | N | B | O |
|---|---|---|---|---|---|---|
| $E - E_v$ (eV) | **1.32** | **2.0** | **0.20** | **2.86** | **0.30** | **2.75** |
| $E_{corr}$ (eV) | **0.91** | | | | | |
| $N_{max}$ (cm$^{-3}$ eV$^{-1}$) | $1.0 \times 10^{18}$ | $3.0 \times 10^{17}$ | $5.0 \times 10^{18}$ | $1.0 \times 10^{19}$ | $1.0 \times 10^{19}$ | $5.0 \times 10^{18}$ |
| Conc. (cm$^{-3}$) | $1.2 \times 10^{16}$ | $3.8 \times 10^{15}$ | $6.3 \times 10^{16}$ | $1.2 \times 10^{17}$ | $1.2 \times 10^{17}$ | $6.3 \times 10^{16}$ |
| $C_n$ (cm$^3$ s$^{-1}$) | **$4.0 \times 10^{-8}$** | **$4.0 \times 10^{-9}$** | $1.0 \times 10^{-12}$ | **$2.0 \times 10^{-13}$** | $1.0 \times 10^{-12}$ | **$5.0 \times 10^{-8}$** |
| $C_p$ (cm$^3$ s$^{-1}$) | **$9.0 \times 10^{-7}$** | $1.0 \times 10^{-8}$ | **$4.5 \times 10^{-12}$** | $1.0 \times 10^{-11}$ | **$1.1 \times 10^{-9}$** | $1.0 \times 10^{-12}$ |

$10^{18}$ cm$^{-2}$ s$^{-1}$ in figure 7(a), and with pw = 1 ms and a photon flux of $10^{17}$ cm$^{-2}$ s$^{-1}$ in figure 7(b). The experimental PITS fringes are presented in figure 1 and the similarity of figure 7 with figure 1 is obvious. On the upper left corner of figure 7(a) one can clearly see the fringe linked to the 'negative' photoconductivity due to the nitrogen level, the PITS amplitude being plotted here with an absolute value. As for the experimental data, the Al level gives rise to a long fringe crossing the figure almost along a diagonal. In figure 7(b) the boron contribution is seen as an 'island' in the middle of the figure. After a close look at the figures, the reader could think that the parameters used in the simulation should have been refined to get a better match between experimental and simulated images. However, as already mentioned, our aim was to understand the main phenomena and not to reproduce the experimental data in every respect.

The reader must note that at this point of the discussion we have reproduced the main experimental features of the PITS experiment. However, if one performs a numerical simulation of the MPC technique with a simple DOS including only Al, B, V, UD1 and N levels, the very high peak at low energy, experimentally found about a thousand times higher than the deep defect peaks (see figure 2(a)), cannot be reproduced. This behaviour can be easily understood by estimating the $NC/\mu$ maximum values that come out of the simulation. As we have seen above, the electrons are the majority carriers so we may just compare the $N_{max}C_n/\mu_n$ quantities for all the levels releasing electrons. Following the data of table 3 one ends with $N_{max}C_n/\mu_n$ for vanadium $N_{max}C_n(V)/\mu_n = 1 \times 10^8$ V cm$^2$ eV$^{-1}$, $N_{max}C_n(\mathrm{UD1})/\mu_n = 3 \times 10^6$ V cm$^2$ eV$^{-1}$ and $N_{max}C_n(\mathrm{N})/\mu_n = 5 \times 10^3$ V cm$^2$ eV$^{-1}$. As in the case of the HRPITS experiment, in MPC the shallower levels are seen at the lower temperatures and therefore the N level should result in a peak at low energy with a lower height than the vanadium one. This is in contradiction with experimental data and to reproduce the very high peak observed in MPC at low energy we have introduced in the numerical simulation a level at 0.25 eV below the conduction band with an electron capture coefficient $C_n = 5 \times 10^{-8}$ cm$^3$ s$^{-1}$ ($\nu = 2.5 \times 10^{11}$ s$^{-1}$). This level corresponds to the one displayed in table 1 that could have been associated with the boron level detected by the PITS experiment. However, this association is probably misleading since it can be seen that neither the energy position nor the attempt-to-escape frequencies are the same for both the levels detected by PITS and MPC. This level was attributed to the presence of oxygen according to other experimental data [20].

In figure 8 we present the r-DOS calculated using the simulated MPC results. The simulation of the MPC experiment was achieved including the oxygen level with the parameters displayed in table 3. The calculations were made from 130 to 700 K with an increment of 10 K. The analogy with the experimental data, and in particular the presence of a very high peak at low energy, is obvious though we obtain a ratio between the maximum r-DOS for shallow and deep levels of only 100 instead of the 1000 that we were seeking. Similarly in the simulation of the PITS experiment, refinement of the simulation parameters could be sought to get a better agreement with the experimental results but it would not bring much more essential information. One can also see, comparing the MPC experimental results (figure 2(b)) and the simulated ones (figure 8), that there is a peak around 1.32 eV found experimentally and not reproduced by the simulation. It means

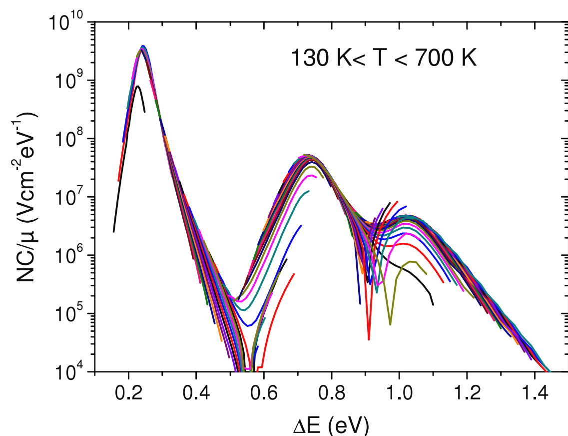


**Figure 8.** Results of a numerical simulation of the MPC experiment with the parameters of the six defect centres given in table 3.

that we should introduce one more level to the six already taken into account, but again it would not bring much more insight into the processes we wanted to highlight.

We can now address some of the questions raised in the comments of the respective MPC and PITS experimental results. The simulation of the photocurrent relaxation in the PITS technique has shown that the majority carriers contributing to the PITS signal are very likely to be the electrons. Nevertheless, their lifetime can be controlled by the hole trapping levels and that is why some defect levels, close to the valence band, can be detected with this technique in the same temperature range in which electron traps are detected. The MPC experiment being sensitive to the majority carrier contribution, here the electrons, implies that the level found experimentally at 0.23–0.25 eV, that we have tentatively identified with boron in table 1, is more likely to be attributed to oxygen. Though being an electron trap, nitrogen is not seen with the MPC technique because its contribution to the $NC/\mu$ value is rather low and masked by the oxygen contribution.

Finally, one can wonder why the oxygen level was not detected by the PITS technique. Two reasons can be invoked. First, in the same temperature range in which nitrogen was detected the simulation has shown that the thermal emission from the O level is likely to happen in a time range much shorter than that of the nitrogen level, i.e. $t < 10\ \mu$s, because of its very high capture coefficient for electrons. Therefore, it was not detected by the PITS technique in the explored temperature range because of the limited bandwidth of the current amplifier. Second, one could then think to lower the temperature to slow down the thermal electron emission rate from the O level. However, the rather low concentration of oxygen, combined with a decrease of the electron lifetime, results in a signal below the limited sensitivity of the current amplifier.

## 5. Conclusions

Electronic properties of defect centres in 6H-SiC crystals have been investigated by means of two different techniques: the photoinduced transient spectroscopy and the modulated photocurrent technique. From the PITS technique, defect levels related to the native UD1 centre, as well as to the impurities such as nitrogen, aluminium, boron and vanadium have been detected. By means of the MPC method, the parameters of some defect levels have also been determined and compared with the PITS results.

A numerical simulation of the time-dependent photoconductivity involved in each experiment was developed to highlight the mechanisms responsible for peculiar experimental features occurring in both techniques such as: (i) 'negative' transient photoconductivity observed in the PITS experiment at low temperature; (ii) contribution to the photocurrent relaxation of both electron and hole traps under the same experimental conditions; (iii) influence of the experimental conditions on the possibility to reveal particular defect levels; (iv) detection with the MPC technique of a defect level that was not put into evidence by the PITS technique.

Numerical simulations of the time dependence of the photocurrent relaxation after the end of the UV pulse have shown that issues (i), (ii) and (iii) are essentially linked to how the occupancy of the levels is achieved during the illumination of the material, as well as on the kinetics of charge carrier emission from various defect levels. Point (iv) was also analysed and explained by means of numerical simulations of the MPC spectra and illustrates the complementarity of both techniques.

As a result of the experimental investigations coupled with numerical simulations, a set of parameters characterizing six different defect centres in 6H-SiC:V has been proposed.

## Acknowledgments

This work was partially supported by EGIDE under contract Polonium 14244QF, as well as by the Polish Ministry of Science and Higher Education within the framework of the Polonium Project no. 7047/R07/R08.

## References

[1] Hurtes C, Boulou M, Mitonneau A and Bois D 1978 *Appl. Phys. Lett.* **32** 821
[2] Benjelloun N, Tapiero M, Zielinger J P, Launay J C and Marsaud F 1988 *J. Appl. Phys.* **64** 4013
[3] Tapiero M, Benjelloun N, Zielinger J P, El Hamd S and Noguet C 1988 *J. Appl. Phys.* **64** 4006
[4] Longeaud C, Kleider J P, Kaminski P, Kozlowski R, Pawlowski M and Cwirko J 1999 *Semicond. Sci. Technol.* **14** 747
[5] Freijlich J, Montenegro R, Innocente Junior N R, dos Santos P V, Launay J C, Longeaud C and Carvalho J F 2007 *J. Appl. Phys.* **101** 043101
[6] Kleider J P and Longeaud C 1995 *Solid State Phenomena* ed H Neber-Aeschbacher (Zurich: Scitec Publication) pp 597–646
[7] Pawlowski M, Kaminski P, Kozlowski R, Jankowski S and Wierzbowski M 2005 *Metrol. Meas. Syst.* **11** 207
[8] Oheda H 1981 *J. Appl. Phys.* **52** 6693
[9] Brüggemann R, Main C, Berkin J and Reynolds S 1990 *Phil. Mag.* B **62** 29
[10] Longeaud C and Kleider J P 1992 *Phys. Rev.* B **45** 11672
[11] Hattori K, Niwano Y, Okamoto H and Hamakawa Y 1991 *J. Non-Cryst. Solids* **137/138** 363
[12] Kaminski P, Kozlowski R, Kozubal M, Zelazko J, Miczuga M and Pawlowski M 2007 *Semiconductors* **41** 414

[13] Kaminski P, Kozlowski R, Miczuga M, Pawlowski M, Kozubal M and Pawlowski M 2008 *J. Mater. Sci.: Mater. Electron* **19** 224

[14] Kaindl W, Lades M, Kaminski N, Niemann E and Wachutka G 1999 *J. Electron. Mater.* **28** 154

[15] Mnatsakanov T T, Levinshtein M E, Pomortseva L I and Yurkov S N 2002 *Semicond. Sci. Technol.* **17** 974

[16] Schneider J and Maier K 1993 *Physica* B **185** 199

[17] Smith S R, Evwaraye A O, Mitchel W C and Capano M A 1999 *J. Electron. Mater.* **28** 190

[18] Harris G L (ed) 1995 *Properties of Silicon Carbide* (London: INSPEC-IEE)

[19] Lebedev A A 1999 *Semiconductors* **33** 107

[20] Dalibor T, Traseger H, Pensl G, Kimoto T, Matsunami H, Nizhner D, Shigiltchoff O and Choyke W J 1999 *Mater. Sci. Eng.* B **61/62** 454

[21] DeOSt at www.lgep.supelec.fr/scm.

[22] Choyke W J 1969 *Mater. Res. Bull.* **4** 141

[23] Longeaud C and Kleider J P 1993 *Phys. Rev.* B **48** 8715

[24] Bubbe R H 1992 *Photoelectronic Properties of Semiconductors* (Cambridge: Cambridge University Press)

[25] Rose A 1966 *Concepts in Photoconductivity and Allied Problems* (New York: Wiley)